Hindawi
Geofluids
Volume 2017, Article ID 4278621, 17 pages
https://doi.org/10.1155/2017/4278621

Research Article

Numerical Investigation into the Impact of CO_2-Water-Rock Interactions on CO_2 Injectivity at the Shenhua CCS Demonstration Project, China

Guodong Yang,[1] Yilian Li,[1] Aleks Atrens,[2] Ying Yu,[1] and Yongsheng Wang[3]

[1]*School of Environmental Studies, China University of Geosciences, Wuhan 430074, China*
[2]*The Queensland Geothermal Energy Centre of Excellence, School of Mechanical and Mining Engineering, The University of Queensland, St Lucia, QLD 4072, Australia*
[3]*China Shenhua Coal Liquefaction Co., Ltd., Ordos 017209, China*

Correspondence should be addressed to Yilian Li; yl.li@cug.edu.cn

Received 25 February 2017; Revised 17 May 2017; Accepted 28 June 2017; Published 3 August 2017

Academic Editor: Tianfu Xu

A 100,000 t/year demonstration project for carbon dioxide (CO_2) capture and storage in the deep saline formations of the Ordos Basin, China, has been successfully completed. Field observations suggested that the injectivity increased nearly tenfold after CO_2 injection commenced without substantial pressure build-up. In order to evaluate whether this unique phenomenon could be attributed to geochemical changes, reactive transport modeling was conducted to investigate CO_2-water-rock interactions and changes in porosity and permeability induced by CO_2 injection. The results indicated that using porosity-permeability relationships that include tortuosity, grain size, and percolation porosity, other than typical Kozeny-Carman porosity-permeability relationship, it is possible to explain the considerable injectivity increase as a consequence of mineral dissolution. These models might be justified in terms of selective dissolution along flow paths and by dissolution or migration of plugging fines. In terms of geochemical changes, dolomite dissolution is the largest source of porosity increase. Formation physical properties such as temperature, pressure, and brine salinity were found to have modest effects on mineral dissolution and precipitation. Results from this study could have practical implications for a successful CO_2 injection and enhanced oil/gas/geothermal production in low-permeability formations, potentially providing a new basis for screening of storage sites and reservoirs.

1. Introduction

Geological storage of carbon dioxide (CO_2) in deep saline formations is widely considered as a significant method for reducing CO_2 emissions in the atmosphere [1, 2]. Currently, a number of CO_2 storage operations and demonstration projects (e.g., Sleipner, Norway, 1996; Weyburn, Canada, 2000; Ketzin, Germany, 2006; Cranfield, USA, 2008; Otway, Australia, 2008) have been conducted around the world [3–7]. The first pilot project of CO_2 capture and storage (CCS) in China, the Shenhua CCS demonstration project, successfully completed its goal of injecting CO_2 at a rate of 100,000 tons/year into the onshore saline aquifer in the Ordos Basin [8]. The site of the Shenhua CCS project is in the Chenjiacun village of Wulam Len town, Ejinhoro county, about 45 km southeast of the Ordos City, Inner Mongolia. The Ordos Basin covers an area of 25×10^4 km^2, is the second largest sedimentary basin in China, and has low porosity and permeability typical of continental basins in China. Deep saline aquifers are widely distributed in the basin, with large potential for CO_2 storage [9]. The Shenhua CCS project used a single vertical well to inject CO_2 into five reservoir-caprock assemblages deeper than 1576 m: the Liujiagou, Shiqianfeng, Shihezi, Shanxi, and Majiagou formations. More than 80% of the total CO_2 injected entered the first three formations [8].

During CO_2 injection at the Shenhua CCS demonstration, a unique phenomenon was observed: the injection index increased nearly tenfold from 4.056 m^3/h/MPa in 2011 to 40.018 m^3/h/MPa in 2013 for the main injection layer, without strong pressure build-up [10]. This indicates that CO_2

injectivity increases after injection started, which is different from earlier predictions [8].

For large-scale injection of CO_2 into saline formations, CO_2 injectivity is a key technical and economic issue of concern. Previous studies and applications show that CO_2 injectivity can be affected by the following mechanisms: (1) pressure build-up due to massive and continuous CO_2 injection; (2) dry-out of the near-well zone due to evaporation of H_2O into unsaturated CO_2; (3) CO_2-water-rock interactions induced by the injection of CO_2 (Bacci et al. 2011) [11–13]. Among these processes, CO_2-water-rock interactions could alter the rock matrix and potentially lead to porosity and permeability changes in the near-well zone [14–17], which is of particular importance for CO_2 injectivity.

Laboratory experiments related to CO_2 injection into sandstone and carbonate rocks have been reported in the previous studies [15, 18–22]. These experiments indicate that CO_2-water-rock interactions can have a substantial effect on porosity and permeability, depending on fluid composition, rock mineralogy, and subsurface thermodynamic conditions. They found that carbonate dissolution processes seem to be the main cause of permeability increases and promote a rapid spreading of the reaction front in short time scales.

Reactive transport modeling has been previously used to investigate geochemical reactions and their effects on permeability and porosity evolution [14, 15, 23–26]. André et al. [14] simulated CO_2 storage in the carbonate-rich Dogger aquifer in the Paris Basin (France) using the reactive transport simulator TOUGHREACT. They found that the porosity in the near-well zone increased significantly due to mineral dissolution. This was in accordance with the reactive flow-through experimental study by Luquot and Gouze [15] for the same basin. Some studies [25, 26] also reported that geochemical reactions dissolved the host rock increasing porosity and permeability thereby affecting fluid flow through reactive transport modeling. On the other hand, Izgec et al. [23] found that CO_2 injection into carbonate aquifers simulated using CMG's STARS could result in permeability reduction as well as improvement depending on the balance between mineral dissolution and precipitation. Furthermore, Sbai and Azaroual [24] found that CO_2 injection could in some circumstances cause particulates to clog reservoir pores leading to a permeability reduction and injectivity decline near the injection well.

Laboratory experiments, imaging characterization, and numerical modeling have previously been combined to describe mineral alteration and associated reactive transport processes and mechanisms in porous media induced by CO_2 injection (Bacci et al. 2011) [16, 27, 28]. Those studies focused on pore- or continuum-scale transport and reaction processes and indicated that CO_2 injectivity increases from dissolution of both carbonate and silicate minerals (especially feldspars). They also confirmed the rapid reaction kinetics of carbonate minerals compared to silicate minerals. Among these research approaches, numerical modeling is an excellent technique in which CO_2 injection and geochemical performance can be modeled at different temporal and spatial scales.

In general, previous studies reveal that CO_2-water-rock interactions induce mineral dissolution and precipitation which can consequently change the porosity and permeability of the subsurface matrix and thus affect the CO_2 injectivity and overall storage capacity. The trend and magnitude of change in porosity and permeability are highly reservoir specific and depend on reservoir properties, which are related to particle sizes, brine composition, and as well the thermodynamic conditions.

Analyses of geohydrological, mechanical, thermal, and geochemical processes involved in Shenhua CCS project have been reported [29–33]. However, few of these have focused on the considerable CO_2 injectivity increase during CO_2 injection period. Liu et al. [33] examined this unique phenomenon through numerical simulation and concluded that it could be explained through heterogeneities in reservoir permeability. However their approach did not consider the possible role of CO_2-water-rock interactions on CO_2 injectivity.

In this study, we applied a 2D radial injection model using the reactive transport code TOUGHREACT to investigate the effect of CO_2-water-rock geochemical reactions on CO_2 injectivity through the evolution of the formation porosity and permeability at the Shenhua CCS site. We focus on Liujiagou, Shiqianfeng, and Shihezi formations, which are the three main formations that sequestrate more than 90% of total CO_2 injected. The goal is to determine the key mechanisms controlling the CO_2-water-rock interactions during CO_2 injection, particularly focusing on investigation of the reasons for CO_2 injectivity improvement in the Shenhua CCS project. Moreover, we examined the impact of various parameters on mineral dissolution/precipitation as well as relevant porosity and permeability changes and compared the simulation results with available experimental data. Understanding of these mechanisms could have important practical implications for a successful CO_2 injection and storage operation in low-permeability formations, providing a new basis for screening of the storage sites and reservoirs and assessing CO_2 injectivity from a geochemical point of view.

2. Modeling Approach

2.1. Numerical Tool. The simulations presented in this study were carried out using the reactive transport code TOUGHREACT [34, 35], which introduces reactive geochemistry into the multiphase fluid and heat flow code TOUGH2 V2 [36]. A fluid property module ECO2N [37] was used to describe isothermal or nonisothermal multiphase flow in H_2O-NaCl-CO_2 system under conditions typically encountered in saline aquifers of interest for CO_2 sequestration ($31^\circ C \leq T \leq 110^\circ C$; $7.38\,MPa < P \leq 60\,MPa$). TOUGHREACT is a thermal-physical-chemical code applicable to one-, two-, or three-dimensional geologic systems with physical and chemical heterogeneity. The numerical method for fluid flow and chemical transport simulation is based on the integral finite difference (IFD) method for space discretization. The system of chemical reaction equations is solved on a grid-block basis by Newton-Raphson iteration. Thermodynamic data used in the simulations were

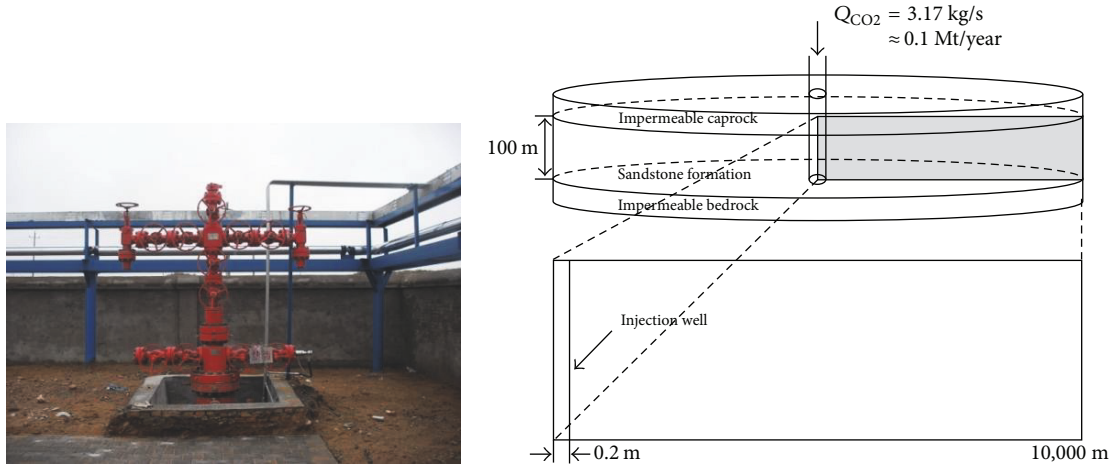

Figure 1: (a) Injection well (Zhongshenzhu 1) at the Shenhua CCS site and (b) schematic diagram of the 2D model.

taken from the EQ3/6 database [38], which derived using SUPCRT92. Local equilibrium constants and kinetic rates used in TOUGHREACT refer to Xu et al. [35].

Porosity changes in the matrix are directly tied to the volume changes as a result of mineral dissolution and precipitation. The porosity of the reservoir in the TOUGHREACT code is calculated by

$$\phi = 1 - \sum_{b=1}^{ab} \mathrm{fr}_b - \mathrm{fr}_u, \tag{1}$$

where ab is the number of minerals; fr_b is the volume fraction of mineral b in the rock ($V_{\mathrm{mineral}}/V_{\mathrm{medium}}$, including porosity); and fr_u is the volume fraction of nonreactive rock.

Reservoir permeability changes are calculated from changes in porosity using ratios of permeabilities as per the Kozeny-Carman grain model [35], as follows:

$$k = k_i \frac{(1-\phi_i)^2}{(1-\phi)^2} \left(\frac{\phi}{\phi_i}\right)^3, \tag{2}$$

where k_i is the initial permeability; ϕ and ϕ_i are current and initial porosity, respectively.

Full details on numerical methods are given in [34, 35].

2.2. Model Description. A two-dimensional (2D) radial model is employed as a conceptual framework to study the CO_2-water-rock interactions on CO_2 injectivity in the three main formations (Liujiagou, Shiqianfeng, and Shihezi) at the Shenhua CCS demonstration project site (Figure 1). The 2D homogeneous model represents a 100 m thick sandstone reservoir with a radial extent of 10 km, sufficiently large to ensure that boundary pressure conditions are maintained constant at initial values, that is, equivalent to an infinitely acting system. Other authors have used similar approximations in previous studies (Bacci et al. 2011) [35, 39]. The grid is composed of 4010 cocentered cell elements. The radius of the first cell containing the injection well is 0.2 m. Away from the injection well, 200 grid cells are considered between 0.2 and 1,000 m, 100 grid cells between 1,000 m and 3,000 m, and 100 grid cells between 3,000 m and 10 km. In each interval, the radius of the cells follows a logarithmic progression. The vertical discretization is achieved by a division of the reservoir into 10 layers with a constant spacing of 10 m. The bedrock and caprock are assumed to be impermeable no-flow boundaries.

CO_2 is injected into the reservoir at a constant flow rate of 3.17 kg/s (corresponding to 0.1 Mt/year) at the bottom 4 layers of the injection well uniformly for 30 years. The physical properties used to model the three formations (which have depth ranges from 1576 m to 2232 m) at the Shenhua CCS site are from previous works [8, 40] and are summarized in Table 1. The initial pressure is in hydrostatic equilibrium determined using the model, and the temperature of the three formations is fixed at 55°C, 62°C, and 67°C, respectively. The porosity and permeability of the three formations are obtained from well log data, and permeabilities are assumed to be isotropic. Pore compressibility of the formations is set to be 4.5×10^{-10}. The capillary pressure and liquid relative permeability are computed by van Genuchten [41], and gas relative permeability is calculated after Corey [42]. Different scenarios have been simulated to determine the different mechanisms of CO_2-water-rock interactions.

2.3. Mineral Composition. The initial rock mineral composition was derived from the laboratory analysis as described in [8, 43–45]. The Liujiagou formation is characterized as feldspar sandstone and lithic arkose. It consists mainly of quartz, alkali feldspar, plagioclase, the multilayer of chlorite and smectite, illite, and kaolinite. The Shiqianfeng formation consists mainly of feldspar rich sandstone and lithic arkose, which is mainly composed of quartz, feldspars, calcite, and small amount of clay minerals (illite and smectite). Feldspathic quartz sandstone and feldspathic lithic sandstone are the main rock type of the Shihezi formation. It consists mainly of quartz with some clay minerals (illite and smectite),

Table 1: Hydrogeological parameters of the formations used in this study.

Parameter	Liujiagou formation	Shiqianfeng formation	Shihezi formation
Permeability (m^2)	2.81×10^{-15}	6.58×10^{-15}	5.99×10^{-15}
Porosity	0.10	0.129	0.126
Pore compressibility (Pa^{-1})	4.5×10^{-10}	4.5×10^{-10}	4.5×10^{-10}
Rock grain density (kg/m^3)	2600	2600	2600
Formation heat conductivity (W/m °C)	2.51	2.51	2.51
Rock grain specific heat (J/kg °C)	920	920	920
Temperature (°C)	55	62	67
Pressure (MPa)	16	18.9	21
Salinity (wt.%)	6	3	0.9
Relative permeability model			
Liquid [41]			
$k_{rl} = \sqrt{S^*}\left\{1 - \left(1 - \left[S^*\right]^{1/\lambda}\right)^{\lambda}\right\}^2$		$S^* = \frac{(S_l - S_{lr})}{(1 - S_{lr})}$	
Residual liquid saturation		$S_{lr} = 0.30$	
Exponent		$\lambda = 0.457$	
Gas [42]			
$k_{rg} = \left(1 - \widehat{S}\right)^2\left(1 - \widehat{S}^2\right)$		$\widehat{S} = \frac{(S_l - S_{lr})}{\left(1 - S_{lr} - S_{gr}\right)}$	
Residual gas saturation		$S_{gr} = 0.05$	
Exponent *capillary pressure model [41]*		$\lambda = 0.457$	
$P_{\text{cap}} = -P_0\left(\left[S^*\right]^{-1/\lambda} - 1\right)^{1-\lambda}$		$S^* = \frac{(S_l - S_{lr})}{(1 - S_{lr})}$	
Residual liquid saturation		$S_{lr} = 0.00$	
Exponent		$\lambda = 0.457$	
Strength coefficient		$P_0 = 19.61$ kPa	

carbonates (calcite and dolomite), and plagioclase. It should be noted that alkali feldspar is represented as K-feldspar, plagioclase is represented as an ideal solid solution of oligoclase, and smectite is divided into Na-smectite and Ca-smectite equally by volume fraction referring to previous studies [46–48]. The detailed mineral composition is given in Table 2.

Simulation results can be influenced profoundly by the choice of secondary mineral assemblage. Almost all possible secondary minerals are considered in the simulations according to previous studies [35, 49].

2.4. Water Geochemistry. The main ions contained in pore water within the three formations are Na^+, Ca^{2+}, and Cl^-; however, the total dissolved solids (TDS) content varies substantially. The Liujiagou formation water is high salinity, with a TDS content of about 56,000 mg/L. The TDS content of Shiqianfeng formation water is 31,200 mg/L, and the TDS content of Shihezi formation water is 9,390 mg/L [44, 45, 50]. Prior to simulating reactive transport, batch geochemical modeling of water-rock interaction was performed to equilibrate the initial formation water composition with the primary formation minerals (Table 2) at the reservoir temperature and CO_2 partial pressure. The background CO_2 partial pressure is chosen to match the measured pH according to Xu et al. [51]. The resulting water chemistry of the three formations (Table 3) is used as the initial conditions for the reactive transport simulation of CO_2 injection.

3. Results and Discussion

3.1. Influence of Porosity and Permeability Changes on CO_2 Injectivity. Injectivity, J, is the flow rate of CO_2 achieved for a particular pressure difference between the injection well and the reservoir. It is linearly proportional to reservoir permeability as given by

$$J = \frac{q}{\Delta P} \propto \frac{2\pi kh}{\mu \ln\left(r_r/r_w\right)}, \tag{3}$$

where q is the volumetric flow rate of injected CO_2, ΔP is a pressure differential between injection pressure and reservoir pressure, h is the vertical thickness of the reservoir, μ is the fluid viscosity, and r is the radial distance with subscripts denoting the well-reservoir interface and boundary of the reservoir. Permeability changes close to the injection well have a comparatively larger effect than permeability changes in distant regions of the reservoir due to the logarithm of radial distance in the denominator. The precise effect of localized changes in permeability can be estimated using an average weighted by the logarithm of the radial distance as defined by

$$\frac{J}{J_i} = \frac{k}{\sum_i^n k_i \ln\left(r_i/r_{i-1}\right)}. \tag{4}$$

For a preliminary analysis of the potential effect of permeability changes, it is not necessary to solve (4) precisely;

Table 2: Mineralogical compositions of the three formations, initial mineral volume fractions introduced in the model, and possible secondary mineral phases used in the simulations.

Mineral	Chemical composition	Volume fraction (%)		
		Liujiagou	Shiqianfeng	Shihezi
Primary				
Quartz	SiO_2	27	65	66
K-feldspar	$KAlSi_3O_8$	14	9	—
Oligoclase	$Ca_{0.2}Na_{0.8}Al_{1.2}Si_{2.8}O_8$	24	16	6
Calcite	$CaCO_3$	—	3	3
Dolomite	$CaMg(CO_3)_2$	—	—	3
Illite	$K_{0.6}Mg_{0.25}Al_{1.8}(Al_{0.5}Si_{3.5}O_{10})(OH)_2$	17	4.5	18.5
Kaolinite	$Al_2Si_2O_5(OH)_4$	6	—	—
Chlorite	$Mg_{2.5}Fe_{2.5}Al_2Si_3O_{10}(OH)_8$	8.5	—	—
Na-smectite	$Na_{0.290}Mg_{0.26}Al_{1.77}Si_{3.97}O_{10}(OH)_2$	1.75	1.25	1.75
Ca-smectite	$Ca_{0.145}Mg_{0.26}Al_{1.77}Si_{3.97}O_{10}(OH)_2$	1.75	1.25	1.75
Total		100	100	100
Secondary:				
Magnesite	$MgCO_3$			
Albite~low	$NaAlSi_3O_8$			
Siderite	$FeCO_3$			
Ankerite	$CaMg_{0.3}Fe_{0.7}(CO_3)_2$			
Dawsonite	$NaAlCO_3(OH)_2$			
Hematite	Fe_2O_3			
Halite	$NaCl$			
Anhydrite	$CaSO_4$			

Table 3: Initial component concentrations of the formation water in the three formations.

Component	Concentration (mol/kg H_2O)		
	Liujiagou	Shiqianfeng	Shihezi
Na^+	1.09	4.19×10^{-1}	1.97×10^{-1}
Ca^{2+}	1.32×10^{-2}	5.66×10^{-2}	2.70×10^{-5}
Mg^{2+}	7.09×10^{-7}	5.59×10^{-13}	2.25×10^{-5}
K^+	6.84×10^{-5}	1.82×10^{-3}	2.87×10^{-5}
Fe^{2+}	1.02×10^{-4}	1.25×10^{-5}	9.52×10^{-11}
Cl^-	1.12	5.06×10^{-1}	1.50×10^{-1}
SO_4^{2-}	3.93×10^{-4}	1.85×10^{-2}	2.26×10^{-7}
HCO_3^-	1.77×10^{-3}	6.50×10^{-4}	4.57×10^{-2}
AlO_2^-	1.32×10^{-8}	2.77×10^{-8}	7.59×10^{-8}
SiO_2 (aq)	5.15×10^{-4}	5.89×10^{-4}	6.63×10^{-4}
pH	7.03	6.68	7.92
Temperature	55°C	62°C	67°C

the order of magnitude of the effect on injectivity can be assessed by assuming a uniform change in permeability. On that basis, injectivity increases linearly with permeability with a gradient of unity. The maximum permeability increases of 0.32%, 0.40%, and 1.39% for the three reservoirs would cause an identical increase in CO_2 injectivity. Consequently the permeability change estimated using (2) and (3) is insufficient to explain the obvious increase in injectivity observed during the Shenhua CCS project.

However, this result relies on the use of the Kozeny-Carman grain model (2) as an estimate of permeability changes in response to porosity change from mineral precipitation/dissolution. Implicit in this model are the assumptions that tortuosity and mineral grain size remain constant as porosity changes, which may not be the case. Furthermore, the Kozeny-Carman model excludes the possibility of a percolation limit to permeability, that is, a minimum porosity below which permeability is zero due to a lack of hydraulic connectivity between pores. Alternative forms of the Kozeny-Carman model have been proposed which account for these factors [52], such as

$$k = k_i \frac{d^2}{d_i^2} \frac{\tau_i^2}{\tau^2} \frac{\left(1 - \phi_i + \phi_p\right)^2}{\left(1 - \phi + \phi_p\right)^2} \frac{\left(\phi - \phi_p\right)^3}{\left(\phi_i - \phi_p\right)^3}, \quad (5)$$

where d represents mineral grain size, τ is tortuosity, and ϕ_p is the percolation porosity for the reservoir rock. From (5), if the CO_2-water-rock interaction-induced mineral dissolution causes grain size increase or tortuosity reduction, it could result in larger permeability increase than calculated from (2).

Grain size does not anticipate increase substantially. Percolation porosity is estimated to typically be 1–3% [52], which is insufficient to explain increases in injectivity: a percolation porosity of 3% would lead to maximum permeability increases of 0.45%, 0.50%, and 1.87% for the three reservoirs. However, tortuosity has been reported to vary widely at fixed porosity for similar rock or other porous medium samples [53]. A large decrease in tortuosity would

cause a very substantial difference in permeability (e.g., a halving of tortuosity would increase permeability by a factor of four). A large decrease in tortuosity can be explained, at least in theory, by mineral precipitation-dissolution that selectively occurs in relation to major fluid flow paths. That is, if dissolution predominates along larger and more direct flow paths, and precipitation mainly occurs in pores that are not part of flow pathways, small changes in total porosity may lead to substantial increase in tortuosity and consequently permeability. Furthermore, it is possible that tortuosity can be decreased by the removal of fine particulates that plug, bridge, or impinge existing or potential fluid flow paths. Only small amounts of dissolution may be necessary to dislodge fines and allow them to settle out of fluid flow.

These possible explanations provide a conceptual framework which could explain injectivity increases in terms of CO_2-water-rock-interaction-induced mineral dissolution and precipitation. Further research would be needed to evaluate whether they are appropriate to apply to this reservoir system. In particular, flow models incorporating fines migration and the effect of mechanical forces on precipitation and dissolution reactions, as well as empirical studies using reservoir core samples, may provide insights into possible geological mechanisms for CO_2 injectivity increase. This further work may assist in differentiating between geochemical changes and permeability heterogeneity as competing explanations for the observed CO_2 injectivity increase.

3.2. Analysis of Mineral Dissolution/Precipitation on Porosity Changes. The amount of dissolution and precipitation of minerals induced by CO_2-water-rock interactions determines porosity change. In order to investigate this process, clarify the key minerals leading to porosity changes, and analyze the differences between different mineral assemblages of the Liujiagou, Shiqianfeng, and Shihezi formations, we investigate the distribution of changes in mineral volume fraction and concentrations of major aqueous species for these three formations along the horizontal direction at the depth of −75 m after 30 years of CO_2 injection.

The change in mineral composition and major aqueous species as a function of CO_2-water-rock interaction-induced dissolution and precipitation for different formations can be seen in Figure 2. Figure 2(a) shows the horizontal distribution of changes in main mineral volume fraction and porosity for Liujiagou formation after 30 years of CO_2 injection. It can be seen that porosity changes throughout the simulation are distinctly tied to the mineral dissolution and precipitation. The spatial distribution of mineral alteration varies in different regions. Mineral dissolution and precipitation are most substantial in zone II because there is sufficient aqueous CO_2 to decrease pH to values as low as 5.0 perturbing the equilibrium state of the system. This is consistent with changes in concentrations of major aqueous species (Figure 2(b)). The main dissolved minerals are oligoclase, chlorite, K-feldspar, and kaolinite, with the oligoclase dissolution providing the main source of volume fraction reduction, in agreement with minerals behavior in laboratory experiments [45]. The main precipitated minerals are Na-smectite, Ca-smectite, illite, and siderite, consuming Ca^{2+} and Mg^{2+} provided by the dissolution of oligoclase and chlorite. The net volume fraction change of minerals is a reduction, resulting in porosity increase.

The resulting porosity changes of the Shiqianfeng formation are explored in Figure 2(c), where the volume fraction changes of minerals versus radial distance are shown after 30 years of CO_2 injection. The injection of CO_2 displaces the liquid flow away from the injection well, but some liquid flow reverses due to capillary-drive, providing water for CO_2-water-rock interactions. The porosity increases slightly in zone I, which can be explained by the large amount of calcite dissolution relative to the anhydrite precipitation. This is consistent with the increase of Ca^{2+} concentration (Figure 2(d)). However, this effect is reduced in the region approximately 30 m away from the well due to many minerals precipitating. In zone II, oligoclase, illite, and calcite volumes decreased relative to initial conditions, while kaolinite, quartz, dawsonite, K-feldspar, Na-smectite, and Ca-smectite volumes increased. Overall, the most important contributor to net volume change caused by precipitation and dissolution was oligoclase dissolution. There was no noticeable change in porosity in zone III because CO_2 has not reached that region of the reservoir.

As shown in Figure 2(e), there is a distinct difference in the mineral alterations between the Shihezi formation and the other two formations, particularly in terms of variation in dolomite and calcite. In the Shihezi formation as the volume fraction of dolomite decreases (6), the volume fraction of calcite increases. This is also demonstrated by the experimental study [44]. The effect of dolomite dissolution and calcite precipitation is substantial in zone I and determines the change in porosity. The changes in this zone can be explained by liquid flow reversal into zone I due to capillary-drive combined with the high reactivity of dolomite resulting in fast CO_2-water-rock interactions. It can be inferred that the dissolution of dolomite provides Ca^{2+} for calcite precipitation ((6)-(7)), with Ca^{2+} making no significant changes (Figure 2(f)). In zone II, the dolomite dissolution and calcite precipitation are also substantial, although the porosity change is also altered by oligoclase dissolution and Na-smectite and Ca-smectite precipitation. The overall effect is a reduction in net mineral volume fraction that leads to porosity increase. Oligoclase dissolution also occurs in zone III, mainly due to precipitation of Na-smectite and Ca-smectite ((8)-(9)), consuming Ca^{2+} and Na^{+} and consequently promoting the dissolution of oligoclase (10):

$$\mathrm{CaMg(CO_3)_2\,(dolomite)} + 2\mathrm{H^+} \longrightarrow \mathrm{Ca^{2+}} + \mathrm{Mg^{2+}} + 2\mathrm{HCO_3^-} \tag{6}$$

$$\mathrm{Ca^{2+}} + \mathrm{HCO_3^-} \longleftrightarrow \mathrm{CaCO_3\,(calcite)} + \mathrm{H^+} \tag{7}$$

$$0.26\mathrm{Mg^{2+}} + 0.29\mathrm{Na^+} + 1.77\mathrm{Al(OH)_3} + 3.97\mathrm{H_4SiO_4} \longrightarrow \mathrm{Na_{0.290}Mg_{0.26}Al_{1.77}Si_{3.97}O_{10}(OH)_2} \cdot (\mathrm{Na-smectite}) + 0.81\mathrm{H^+} + 9.19\mathrm{H_2O} \tag{8}$$

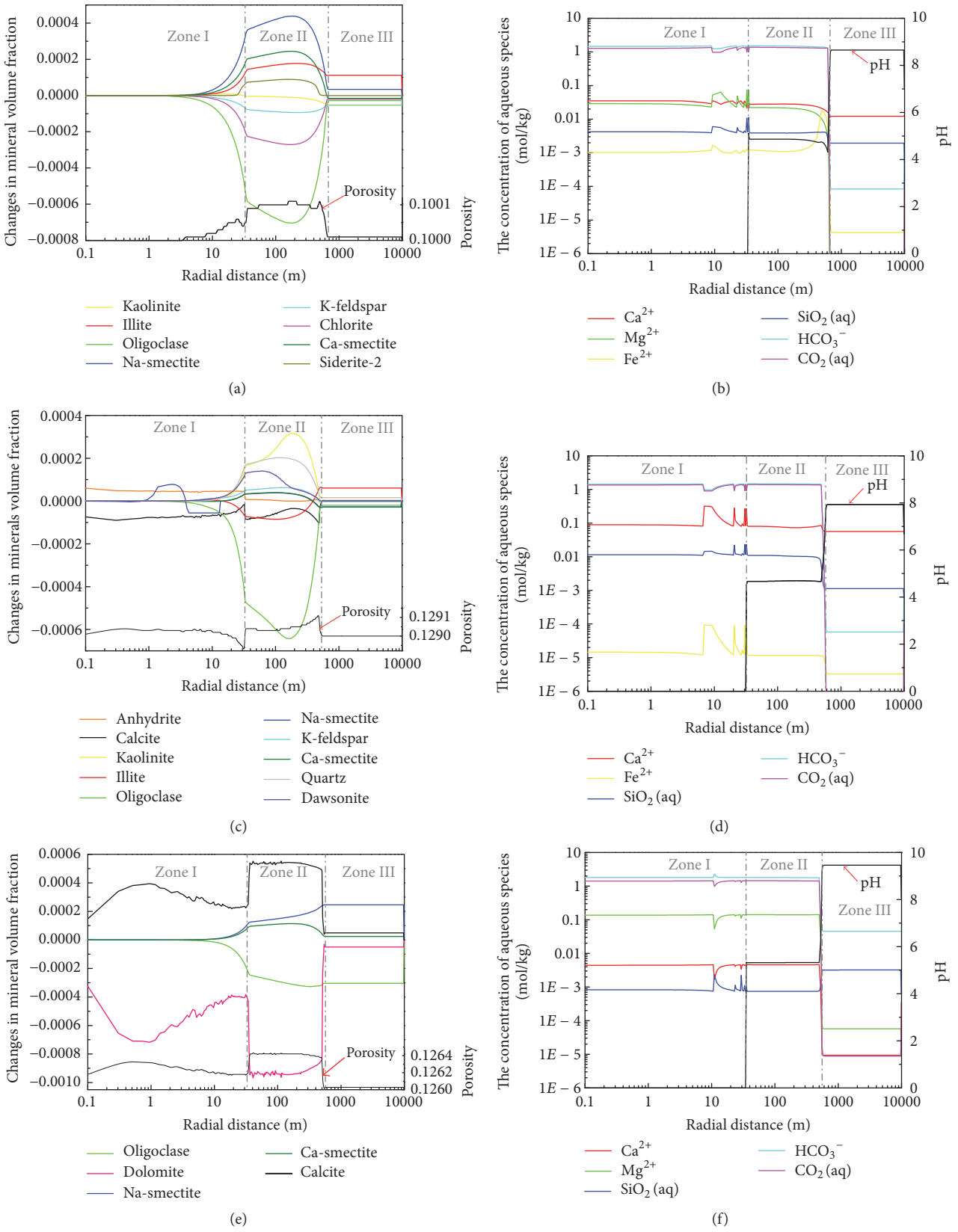

FIGURE 2: The horizontal distribution of changes in main mineral volume fraction, porosity, and concentrations of major aqueous species and pH for Liujiagou formation (a, b), Shiqianfeng formation (c, d), and Shihezi formation (e, f) along the horizontal direction at the depth of −75 m after 30 years of CO_2 injection.

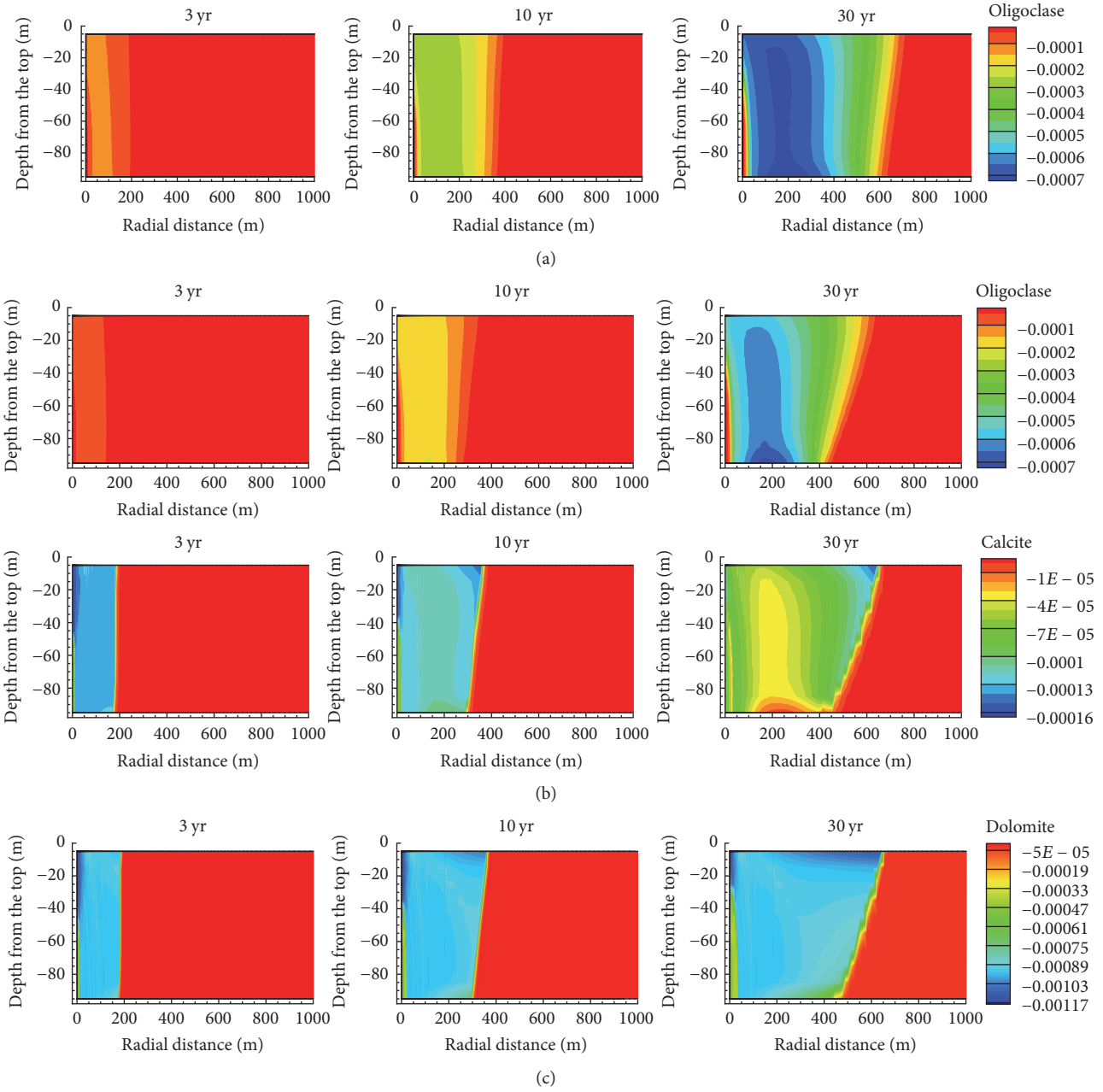

Figure 3: Temporal and spatial evolution of the key minerals volume fraction in the three formations ((a) Liujiagou formation; (b) Shiqianfeng formation; (c) Shihezi formation).

$$0.26Mg^{2+} + 0.145Ca^{2+} + 1.77Al(OH)_3 + 3.97H_4SiO_4 \longrightarrow Ca_{0.145}Mg_{0.26}Al_{1.77}Si_{3.97}O_{10}(OH)_2 \cdot (Ca-smectite) + 0.81H^+ + 9.19H_2O \quad (9)$$

$$CaNa_4Al_6Si_{14}O_{40}(Oligoclase) + 6H^+ + 34H_2O \longrightarrow Ca^{2+} + 4Na^+ + 6Al(OH)_3 + 14H_4SiO_4 \quad (10)$$

The temporal and spatial evolution of the volume fraction of key minerals within the three formations is shown in Figure 3. By analyzing the porosity changes and mineral alteration in Figures 2 and 3, it can be seen that the key minerals affecting porosity in the near-well region (zone I) are calcite and dolomite. In zone II, the dissolution of oligoclase and dolomite plays the key role in porosity increases, which is consistent with the phenomenon observed by Hao et al. [16] through the study of CO_2-induced dissolution processes of low-permeability carbonate reservoirs. It can be concluded that oligoclase, dolomite, and calcite are the key minerals that

Table 4: Summary of the simulation cases.

Simulation scenarios	Variable changed	Alternative value
Case 1	Dolomite volume fraction (%)	0
Case 2		15
Case 3	Calcite volume fraction (%)	0
Case 4		15
Case 5	Oligoclase volume fraction (%)	0
Case 6		15
Case 7	Temperature (°C)	50
Case 8		80
Case 9	Pressure (MPa)	10
Case 10		30
Case 11	Salinity (wt.%)	0.09
Case 12		9
Case 13		15

affect porosity increases in the Shenhua CCS demonstration project during CO_2 injection.

These results indicate the importance of localized mineral dissolution during CO_2-water-rock interactions, which can lead to a large increase in the volume of void space thereby increasing the porosity and permeability of the reservoir, and potentially CO_2 injectivity via mechanisms previously discussed.

3.3. Analysis of Factors Affecting Porosity Change. Mineral composition, temperature, pressure, and salinity may each influence CO_2-water-rock interactions (mineral dissolution/precipitation) thereby affecting porosity and permeability changes. In order to investigate the influence of these factors, an additional 13 simulation cases were analyzed, each varying one factor relative to a base case for the Shihezi formation (Table 4). It should be noted that the mineral composition (especially dolomite, calcite, and oligoclase) and formation physical properties (e.g., temperature, pressure, and brine salinity) are the key difference between the different formations. Therefore, a series of analyses are conducted to assess how the porosity and permeability changes and mineral alteration are affected by these parameters.

3.3.1. Impacts of Key Minerals. Dolomite is one of the key primary minerals in the system. Figures 4(a) and 4(b) show the difference in the porosity change and mineral alteration if the reservoir contains larger or smaller amounts of dolomite. It can be seen that the maximum porosity is above 12.61% in the CO_2 plume when there is no dolomite in the system. The maximum porosity increases to 12.645% when the initial volume fraction of dolomite is 3%. However, when the initial volume fraction of dolomite is 15%, porosity is not markedly increased, and in fact porosity changes in zone II coincide with results for a dolomite volume fraction of 3%. As dolomite content increases in the near-well region (zone I), it has less effect on porosity change; this is because reactivity is limited by lack of water (due to evaporation of water into the free CO_2 phase) and excessive initial mineral (i.e., dolomite supersaturation). This was also observed in a flow-through experiment performed by Tutolo et al. [22].

The complex effect of dolomite on the porosity results from the different behavior of minerals alteration induced variation in dolomite content. As shown in Figures 4(b) and 4(c), when there is no dolomite in the system, the minerals and major aqueous species show very different behavior compared with the base case. Under those circumstances, calcite is dissolved rather than precipitated in zone I and zone II, and oligoclase mainly dissolves in zone II, while there is no Mg^{2+} provided by dolomite. Some kaolinite and quartz precipitated, which is also very different from the base case.

The overall effect of increased dolomite volume fraction is a reduction in net mineral volume fraction, leading to a minor porosity increase. When dolomite is present (and consequently Ca^{2+} and Mg^{2+}), dedolomitization occurs: dolomite transforms into calcite. This result agrees well with Yan and Zhang's study [54]. It occurs because the change in Gibbs free energy (ΔG) for dolomite dissolution is smaller than that for calcite dissolution; that is, the required energy for dolomite dissolution is less than that for calcite [27, 55]. Consequently the dissolution of dolomite occurs more readily than that of calcite. Furthermore, the presence of dolomite can promote the precipitation of Na-smectite and Ca-smectite and the dissolution of oligoclase outside the CO_2 plume.

Compared with dolomite, calcite has minimal effects on the mineral alteration, porosity, and major aqueous species changes in the system, as shown in Figures 4(d)–4(f). It should be noted that the black line representing 3% volume fraction calcite coincides with the blue line representing 15% calcite. When calcite is absent in the primary minerals, calcite is still precipitated in the system, due to the increase in Ca^{2+} supplied by dolomite dissolution (dedolomitization) mentioned above. Only when dolomite is absent can calcite dissolve to make a contribution to the porosity increase (Figures 2(c) and 4(b)).

Figures 4(g)–4(i) show the changes in major aqueous species, porosity, and relevant mineral alteration with respect to radial distance for different initial oligoclase content. These results indicate that oligoclase also plays an important role in porosity and permeability changes (Figure 4(g)). It can be seen that the greater the oligoclase content, the smaller the porosity increases and the concentration of Mg^{2+} supplied by dolomite, which is mainly because oligoclase can inhibit the dissolution of dolomite (Figure 4(h)). This further suggests that dolomite is an important mineral for formation porosity increases and CO_2 injectivity improvement.

3.3.2. Impacts of Physical Parameters. In order to investigate the impact of physical parameters, temperature, pressure, and salinity, we have used the Shihezi formation as the base case to vary one factor to obtain the temperature, pressure, and salinity targeted allowing more comparable, consistent, and making sense results. The initial temperature and pressure of the Shihezi formation are 67°C and 21 MPa, and the variation of temperature is 50°C (Case 7) and 80°C (Case 8), and the pressure is 10 MPa (Case 9) and 30 MPa (Case 10). The initial

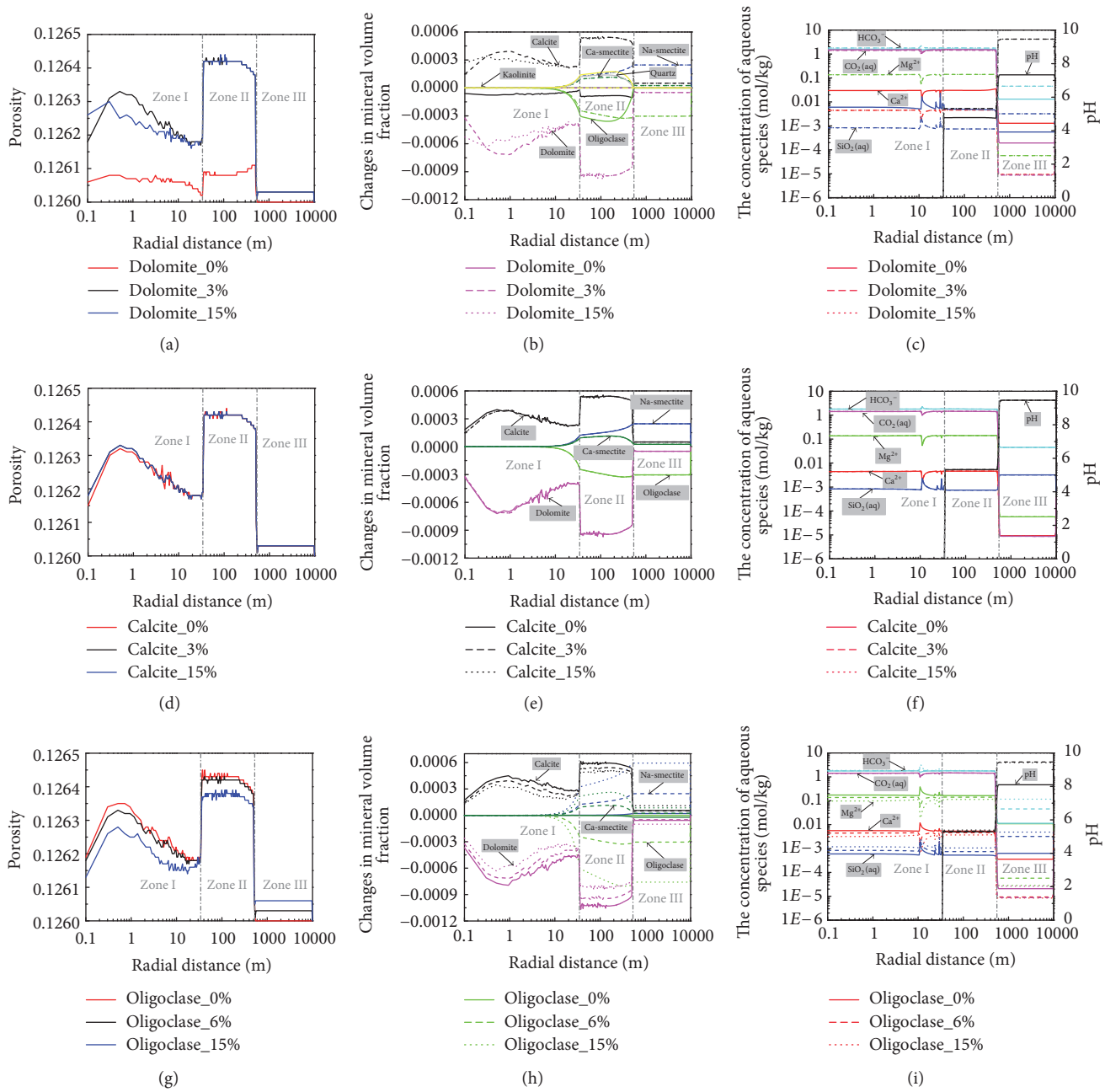

FIGURE 4: The horizontal distribution of changes in porosity, mineral volume fraction, and concentrations of major aqueous species and pH for different amounts of dolomite (a, b, and c), calcite (d, e, and f), and oligoclase (g, h, and i) at the depth of −75 m after 30 years of CO_2 injection.

water salinity of the Shihezi formation is 0.9 wt.% dissolved NaCl, and it is evaporated to 9 (Case 12) and 15 (Case 13) wt.% dissolved NaCl and diluted to 0.09 wt.% dissolved NaCl (Case 11) to evaluate the salinity effect, as can be seen in Table 4.

Temperature. Figure 5(a) shows that the porosity change at the reservoir temperature of 67°C is larger than at the temperature of 50°C and 80°C, indicating that the changes in porosity increase first and then decrease with increasing reservoir temperature in zone I and zone II, with the maximum value occurring between 50°C and 80°C. This is attributed to the changes in mineral volume fraction that the dissolution of dolomite increases first and then decreases with increasing temperature in zone I and zone II (Figure 5(b)), which is consistent with the study conducted by Yan et al. [56]. Although the dissolution of oligoclase increases with increasing temperature, the precipitation of Na-smectite and Ca-smectite increases correspondingly in zone II, such that there is nearly no net contribution to porosity increases. Porosity increases with larger temperatures in zone III without CO_2, resulting

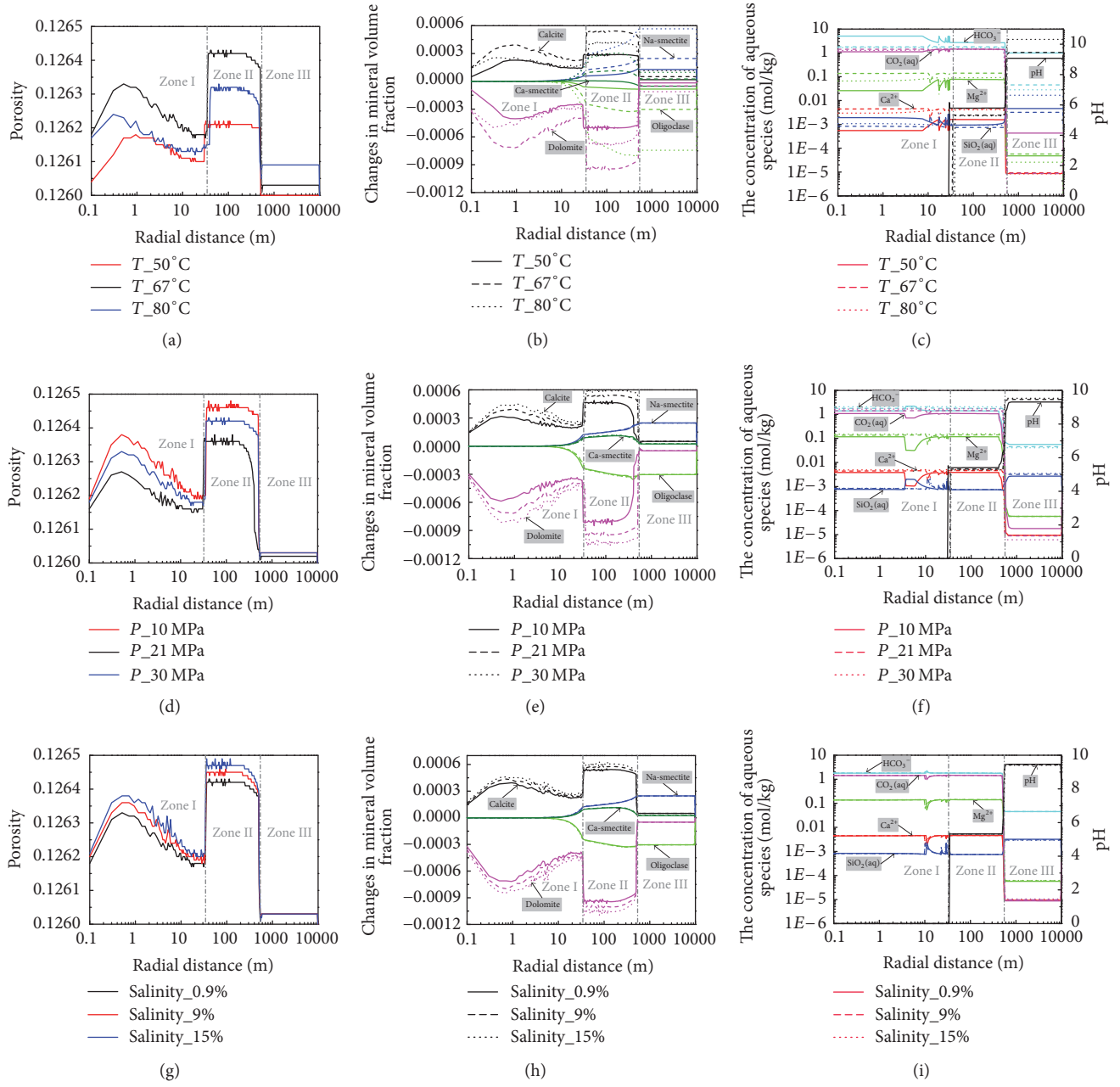

FIGURE 5: The horizontal distribution of changes in porosity, mineral volume fraction, and concentrations of major aqueous species and pH for different temperature (a, b, and c), pressure (d, e, and f), and salinity (g, h, and i).

from the dissolution of oligoclase. The effect of temperature on the horizontal distribution of changes in major aqueous species is shown in Figure 5(c), which agrees well with the mineral alteration. It can be concluded that temperature has a large effect on mineral dissolution and precipitation as well as consequent porosity and permeability changes.

Pressure. The impact of pressure on the horizontal distribution of changes in porosity, mineral volume fraction, and major aqueous species is shown in Figures 5(d)–5(f). It can be seen that the change in porosity increases with increasing pressure from 10 MPa to 30 MPa (Figure 5(d)). However, the impact of pressure on the precipitation and dissolution of different minerals varies. This also leads to the complex behavior of major aqueous species (Figure 5(f)). The dissolution of dolomite increases with pressure resulting in corresponding calcite precipitation, while no effect of pressure on oligoclase dissolution is observed within the pressure range investigated. This also supports the idea that the porosity increases resulted from the key carbonate mineral-dolomite dissolution.

Salinity. The effect of salinity on porosity was evaluated by evaporating the initial water of the Shihezi formation

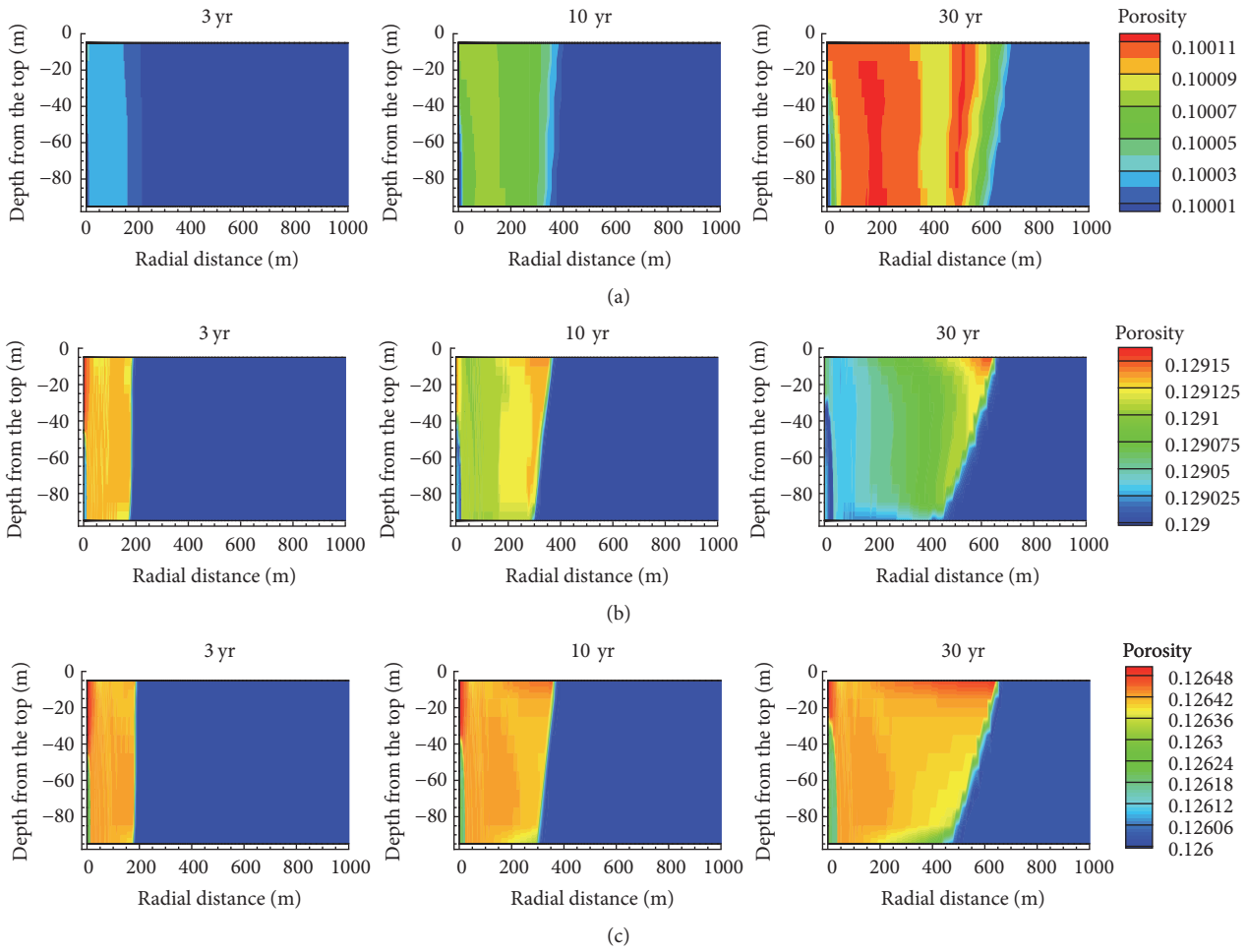

Figure 6: The evolution of porosity in the three formations ((a): Liujiagou formation; (b): Shiqianfeng formation; (c): Shihezi formation).

(0.9 wt.% dissolved NaCl) to increase salinity to 9 and 15 wt.% dissolved NaCl and diluting the initial water to decrease the salinity to 0.09 wt.% dissolved NaCl. As shown in Figure 5(g), the changes in porosity increase with salinity between 0.9 and 15 wt.% dissolved NaCl. It can be inferred that the overall effect of salinity is a reduction in net mineral volume fraction. Figures 5(h) and 5(i) show the horizontal distribution of changes in mineral volume fraction and major aqueous species, which demonstrate this. It can be seen that the dissolution of dolomite increases with increasing salinity, while the dissolution-precipitation of other minerals and major aqueous species does not change except for minor calcite precipitation. This is in accordance with previous studies [22, 54] and can be explained by the ionic strength of the solution increasing with salinity and reducing the activity of aqueous species, thereby promoting dolomite dissolution. There was no obvious difference in the porosity changes between salinities of 0.09% (not shown) and 0.9 wt.% dissolved NaCl. This is probably because both those salinities are so low that there is no significant effect on mineral alteration and consequent porosity changes.

3.4. Temporal and Spatial Evolution of Porosity and Permeability. The injection of CO_2 into the deep saline aquifers results in a sequence of CO_2-water-rock interactions, inducing mineral dissolution and precipitation, which can have a substantial impact on the porosity and permeability of the reservoir. Figure 6 shows the evolution of porosities in the Liujiagou, Shiqianfeng, and Shihezi formations. Porosity within each formation increases gradually with time, and the variation range of porosity is consistent with the migration scope of CO_2; this is consistent with the field observations [8]. However, the distribution of porosities is nonuniform in the range of CO_2 plume. This might be due to different geochemical reactions in different regions. The three reservoirs experienced increases in porosity of up to 0.10%, 0.12%, and 0.42%, respectively, depending on the primary mineral compositions and reservoir conditions.

Figure 7 shows the temporal and spatial evolution of permeability in the Liujiagou, Shiqianfeng, and Shihezi formations. The three formations experienced increases in permeability of up to 0.32%, 0.40%, and 1.39%. The variations in permeability agree with those of porosity (Figure 6),

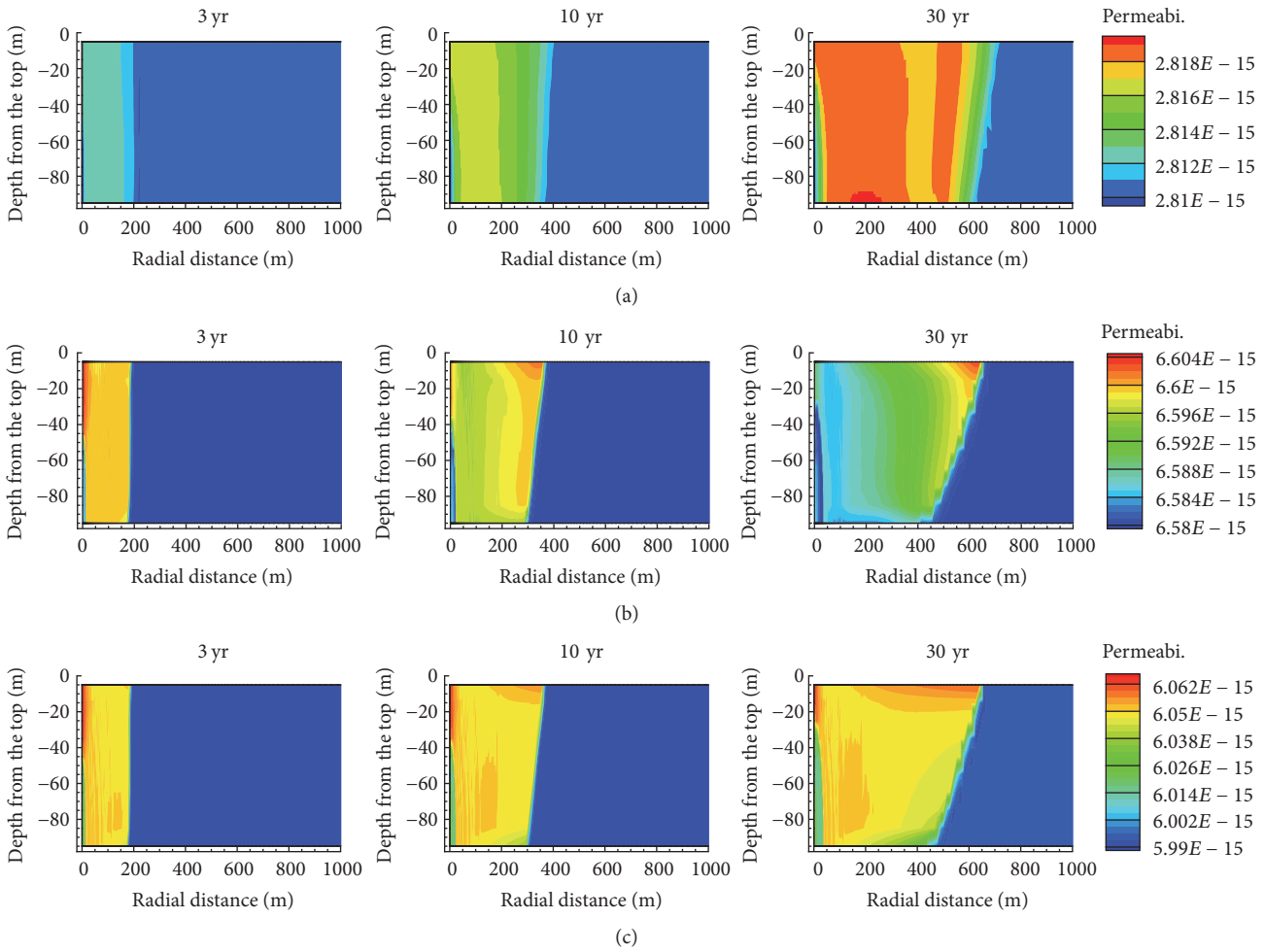

FIGURE 7: The evolution of permeability in the three formations ((a): Liujiagou formation; (b): Shiqianfeng formation; (c): Shihezi formation).

because that permeability is calculated from porosity using (2).

The supercritical CO_2 saturation and nonuniform distribution of porosity change along the horizontal direction at the depth of −75 m after 30 years of CO_2 injection are shown in Figure 8. It can be seen that the distribution of reservoir porosity is closely related to the change of supercritical CO_2 saturation. The reservoir system could be divided into three regions according to supercritical CO_2 saturation, which are (1) zone I: supercritical CO_2 region, where all the water has been displaced or has evaporated and Sg is close to one, (2) zone II: CO_2 and saline water region, where the pH decreases due to CO_2 dissolution in the water phase and stabilizes at a pseudoequilibrium value of approximately 5.0, and (3) zone III: saline water region, consisting of formation waters undisturbed by injected CO_2. The distribution of porosity change corresponds to these three distinct regions of supercritical CO_2 saturation (Figure 8). Porosity changes are different between the three formations due to their different physical and chemical properties and the corresponding balance of mineral dissolution and precipitation induced by CO_2-water-rock interactions.

The porosity change in the Liujiagou formation is the most limited: it increases slightly within zone I at distances of more than 3 m from the injection well, and there is a moderate uniform increase in porosity in zone II. In zone III, the porosity does not change because the system maintains its initial equilibrium state without CO_2 disturbance. The changes in porosity of the Shiqianfeng formation are slightly larger than Liujiagou formation, and the variation trend is different in each region, especially in zone I. Among the three formations, the changes in porosity of the Shihezi formation are largest, with the maximum changes located in zone II.

The CO_2-water-rock interactions after CO_2 injection lead to changes in porosity and permeability. These changes are directly tied to mineral dissolution and precipitation, calculated by (1)-(2) [35]. If the volume of minerals dissolved is larger than the volume of those precipitated, a porosity increase results. This will lead to an increase in permeability, which consequently enhances the injectivity of CO_2 into the formation. The differences in porosity changes between the three formations indicate that different CO_2-water-rock interactions occur in the Liujiagou, Shiqianfeng, and Shihezi formations. It can be concluded that porosity changes of zone

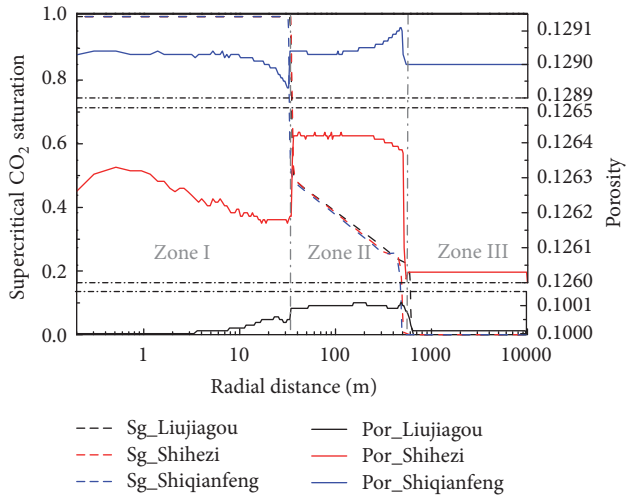

FIGURE 8: The distribution of porosity and supercritical CO_2 saturation in the horizontal plane at the depth of −75 m after 30 years of CO_2 injection in the three formations.

II are larger than those in zone I. This is mainly because no condensed water is present in zone I and consequently mineral reactions are limited, while zone II is a two-phase region with sufficient saline water and CO_2 for CO_2-water-rock reactions to proceed rapidly.

3.5. Comparison with Laboratory Experiments and Previous Other Modeling Work. With regard to Shenhua CCS demonstration project, the CO_2-water-rock interactions and associated mineral dissolution/precipitation after CO_2 injection have been tested in laboratory experiments [43–45] and we find good qualitative agreement with our results. Tao [45] conducted batch reaction experiments with sandstone using a mixture of CO_2 and brine fluids at temperatures of 60°C, 80°C, and 100°C and a pressure of 16 MPa for 1 to 25 days. The sandstone samples were sourced from the Liujiagou group at the Shenhua CCS demonstration project site. After the dissolution of CO_2, SEM and EDS analyses showed significant dissolution of primary minerals such as K-feldspar, albite, and chlorite and precipitation of secondary minerals such as siderite and some clay minerals. It should be noted that albite here is corresponding to oligoclase in our studies. These mineral alteration patterns are well consistent with our simulations.

Batch reactions were also conducted by Wang [43] and Yang [44] using sandstone samples from the Shiqianfeng formation and Shihezi formation, Ordos Basin, China. The experiments were conducted for 24 days at temperatures of 55°C, 70°C, 85°C, and 100°C and the same pressures of 18 MPa. SEM and EDS analyses showed albite and carbonates such as calcite and dolomite dissolved following the decrease of pH after CO_2 injection. During the experiment, the dissolution of carbonates buffered the fluid pH between 5 and 7.3. The concentration of K^+, Na^+, and Ca^{2+} increased due to the dissolution of initial dolomite and albite. Their findings on the amount of minerals alteration are in general agreement with our simulations, in which the dissolution of minerals is larger than the precipitation, and mineral dissolution amount increased with increasing temperature in a certain temperature range. This can explain field observations well that the injectivity increased after CO_2 injection.

The experiments discussed showed there were only intermediate states of carbonate minerals and some unknown aluminosilicate minerals precipitated, and the precipitation of clay minerals was rarely observed. This is in contrast to our simulation results where precipitation of carbonates such as dawsonite and calcite and clay minerals such as smectite and kaolinite precipitation associated with oligoclase dissolution were predicted. The differences are explained by factors such as kinetic and nucleation effects that likely prevent the formation of these minerals over the short time scales (only 24 days) of the laboratory experiments [44, 57].

In addition to batch experiments discussed above, we have also compared our results with previous reactive transport modeling results [39, 57, 58]. These simulations suggested that mineral dissolution and precipitation induced by CO_2 injection have a major impact on the porosity and permeability changes. Liu et al. [58] performed coupled reactive flow and transport modeling of CO_2 injection in the Mt. Simon sandstone formation, Midwest USA. They found dissolution of K-feldspar, oligoclase, and dolomite originating in the matrix caused increase in porosity, from the original 15% to 15.7% in the near-well zone during the injection period, which is in line with our simulation. In another recent paper [57], the initial mineral composition used in this work was similar with Shiqianfeng formation in our studies, but the minerals contents and in situ conditions (e.g., temperature and pressure) are different. Despite these differences, their results are well consistent with our studies that the increase in porosity is caused by the acidic brine that triggered the dissolution of minerals such as calcite and albite (corresponding to oligoclase in our studies). Also, the formation of dawsonite was observed in both models.

4. Conclusions

This study investigated CO_2-water-rock geochemical reactions during CO_2 injection at the Shenhua CCS demonstration site using two-dimensional (2D) reactive transport model. The potential role of mineral dissolution and precipitation (and resulting porosity change) in explaining the nearly tenfold increase in injectivity observed at that site was explored using conventional and alternative porosity-permeability models. The effect on mineral dissolution/precipitation of key mineral composition (e.g., dolomite, calcite, and oligoclase) and formation physical properties (e.g., temperature, pressure, and brine salinity) was also examined. The conclusions are as follows.

The CO_2-water-rock interactions induced by CO_2 injection into the deep saline aquifers affect the porosity evolution of the reservoir due to mineral dissolution and precipitation. The porosities of the three formations increase gradually over time during CO_2 injection, and the spatial distribution of porosity change is consistent with the migration scope of CO_2. The porosities of the Liujiagou, Shiqianfeng, and Shihezi reservoirs experienced maximum increases of 0.10%,

0.12%, and 0.42%, respectively. The differences in porosity changes between these three formations are a consequence of the different CO_2-water-rock interactions occurring due to their different primary mineral compositions and reservoir conditions.

The reservoir permeability will increase as a consequence of the porosity increase. Using a typical Kozeny-Carman porosity-permeability relationship, the nearly tenfold injectivity increase observed cannot be attributed to CO_2-water-rock interaction-induced mineral dissolution. However, using porosity-permeability relationships that include tortuosity, grain size, and percolation porosity, it is possible to explain the injectivity increase as a consequence of mineral dissolution. These models might be justified in terms of selective dissolution along flow paths and by dissolution or migration of plugging fines. Empirical studies using core samples would be necessary to evaluate the suitability of applying these alternative models to the Shenhua CCS site. Further research could also explore the near-wellbore porosity-permeability changes at the early stage of CO_2 injection and also as to whether more extreme variations in reservoir properties could explain permeability changes under a Kozeny-Carman porosity-permeability relationship.

Variation of key mineral composition and physical reservoir parameters illustrates that dolomite is the key mineral that affects porosity increase during CO_2 injection, and the dissolution of dolomite can inhibit the dissolution of calcite. The dissolution of oligoclase can also lead to porosity increase, although oligoclase can also inhibit the dissolution of dolomite, which is not conducive to porosity increase. Formation physical properties such as temperature, pressure, and brine salinity are all important factors that affect mineral dissolution and precipitation as well as relevant porosity and permeability changes.

The simulation results are compared with available experimental data and found to show reasonably good agreement. These results indicate the importance of localized mineral dissolution during CO_2-water-rock interactions, which can lead to a large increase in the volume of void space thereby increasing the porosity and permeability of the reservoir. This study helps deepen our understanding of how geochemical changes may affect CO_2 injectivity. Results from this study could have important practical implications for a successful CO_2 injection and enhanced oil/gas/geothermal production in low-permeability formations, providing a new basis for screening of the most effective storage sites and reservoirs and assessing CO_2 injectivity by considering specific mineralogy and in situ conditions.

Conflicts of Interest

The authors declare that there are no conflicts of interest regarding the publication of this paper.

Acknowledgments

This work was supported by the National Natural Science Foundation of China (NSFC, Grant nos. 41602272 and 41572233), a bilateral project China Australia Geological Storage of CO2 Project Phase 2 (CAGS2), and the project funded by China Postdoctoral Science Foundation (Grant no. 2016M592405).

References

[1] S. Bachu, "Sequestration of CO_2 in geological media in response to climate change: Road map for site selection using the transform of the geological space into the CO_2 phase space," *Energy Conversion and Management*, vol. 43, no. 1, pp. 87–102, 2002.

[2] IPCC, "IPCC Special Report on carbon dioxide capture and storage," in *Prepared by Working Group III of the Intergovernmental Panel on Climate Change*, p. 442, Cambridge University Press, Cambridge, UK, 2005.

[3] P. J. Cook, "Demonstration and Deployment of Carbon Dioxide Capture and Storage in Australia," in *Proceedings of the 9th International Conference on Greenhouse Gas Control Technologies, GHGT-9*, pp. 3859–3866, November 2008.

[4] C. Hermanrud, T. Andresen, O. Eiken et al., "Storage of CO_2 in saline aquifers-Lessons learned from 10 years of injection into the Utsira Formation in the Sleipner area," *Energy Procedia*, vol. 1, pp. 1997–2004.

[5] S. Whittaker, B. Rostron, C. Hawkes et al., "A decade of CO_2 injection into depleting oil fields: monitoring and research activities of the IEA GHG Weyburn-Midale CO_2 Monitoring and Storage Project," *Energy Procedia*, vol. 4, pp. 6069–6076, 2011.

[6] J. Lu, Y. K. Kharaka, J. J. Thordsen et al., "CO_2—rock—brine interactions in Lower Tuscaloosa Formation at Cranfield CO_2 sequestration site, Mississippi, U.S.A," *Chemical Geology*, vol. 291, pp. 269–277, 2012.

[7] T. Kempka and M. Kühn, "Numerical simulations of CO_2 arrival times and reservoir pressure coincide with observations from the Ketzin pilot site, Germany," *Environmental Earth Sciences*, vol. 70, pp. 3675–3685, 2013.

[8] X. Wu, *Carbon Dioxide Capture and Geological Storage: The First Massive Exploration in China*, Beijing, Science Press, Beijing, China, 2013.

[9] Q. Li, G. Liu, X. Liu, and X. Li, "Application of a health, safety, and environmental screening and ranking framework to the Shenhua CCS project," *International Journal of Greenhouse Gas Control*, vol. 17, pp. 504–514, 2013.

[10] China Shenhua Coal to Liquid and Chemical Engineering Company, *The operation report of the Shenhua 0.1 Mt CCS Demonstration Project*, 2014.

[11] T. A. Buscheck, Y. Sun, M. Chen et al., "Active CO_2 reservoir management for carbon storage: Analysis of operational strategies to relieve pressure buildup and improve injectivity," *International Journal of Greenhouse Gas Control*, vol. 6, pp. 230–245, 2012.

[12] L. André, Y. Peysson, and M. Azaroual, "Well injectivity during CO_2 storage operations in deep saline aquifers - Part 2: Numerical simulations of drying, salt deposit mechanisms and role of capillary forces," *International Journal of Greenhouse Gas Control*, vol. 22, pp. 301–312, 2014.

[13] Q. Li, Y.-N. Wei, G. Liu, and Q. Lin, "Combination of CO_2 geological storage with deep saline water recovery in western China: Insights from numerical analyses," *Applied Energy*, vol. 116, pp. 101–110, 2014.

[14] L. André, P. Audigane, M. Azaroual, and A. Menjoz, "Numerical modeling of fluid-rock chemical interactions at the supercritical CO_2-liquid interface during CO_2 injection into a carbonate reservoir, the Dogger aquifer (Paris Basin, France)," *Energy Conversion and Management*, vol. 48, pp. 1782–1797, 2007.

[15] L. Luquot and P. Gouze, "Experimental determination of porosity and permeability changes induced by injection of CO_2 into carbonate rocks," *Chemical Geology*, vol. 265, pp. 148–159, 2009.

[16] Y. Hao, M. Smith, Y. Sholokhova, and S. Carroll, "CO_2-induced dissolution of low permeability carbonates. Part II: Numerical modeling of experiments," *Advances in Water Resources*, vol. 62, pp. 388–408, 2013.

[17] G. P. D. De Silva, P. G. Ranjith, and M. S. A. Perera, "Geochemical aspects of CO_2 sequestration in deep saline aquifers: A review," *Fuel*, vol. 155, pp. 128–143, 2015.

[18] C. F. J. Colón, E. H. Oelkers, and J. Schott, "Experimental investigation of the effect of dissolution on sandstone permeability, porosity, and reactive surface area," *Geochimica et Cosmochimica Acta*, vol. 68, pp. 805–817, 2004.

[19] O. Izgec, B. Demiral, H. Bertin, and S. Akin, "CO_2 injection into saline carbonate aquifer formations I: Laboratory investigation," *Transport in Porous Media*, vol. 72, pp. 1–24, 2008.

[20] M. M. Smith, Y. Sholokhova, Y. Hao, and S. A. Carroll, "CO_2-induced dissolution of low permeability carbonates. Part I: Characterization and experiments," *Advances in Water Resources*, vol. 62, pp. 370–387, 2013.

[21] A. J. Luhmann, X.-Z. Kong, B. M. Tutolo et al., "Experimental dissolution of dolomite by CO_2-charged brine at 100∘C and 150 bar: Evolution of porosity, permeability, and reactive surface area," *Chemical Geology*, vol. 380, pp. 145–160, 2014.

[22] B. M. Tutolo, A. J. Luhmann, X. Kong, M. O. Saar, and W. E. Seyfried, "Experimental Observation of Permeability Changes In Dolomite at CO_2 Sequestration Conditions," in *Environmental Science & Technology*, vol. 48, pp. 2445–2452, 2014.

[23] O. Izgec, B. Demiral, H. Bertin, and S. Akin, "CO_2 injection into saline carbonate aquifer formations II: Comparison of numerical simulations to experiments," *Transport in Porous Media*, vol. 73, pp. 57–74, 2008.

[24] M. A. Sbai and M. Azaroual, "Numerical modeling of formation damage by two-phase particulate transport processes during CO_2 injection in deep heterogeneous porous media," *Advances in Water Resources*, vol. 34, pp. 62–82, 2011.

[25] S. Sadhukhan, P. Gouze, and T. Dutta, "Porosity and permeability changes in sedimentary rocks induced by injection of reactive fluid: A simulation model," *Journal of Hydrology*, vol. 450-451, pp. 134–139, 2012.

[26] J. P. Nogues, J. P. Fitts, M. A. Celia, and C. A. Peters, "Permeability evolution due to dissolution and precipitation of carbonates using reactive transport modeling in pore networks," *Water Resources Research*, vol. 49, pp. 6006–6021, 2013.

[27] S. Molins, D. Trebotich, L. Yang et al., "Pore-scale controls on calcite dissolution rates from flow-through laboratory and numerical experiments," *Environmental Science & Technology*, vol. 48, pp. 7453–7460, 2014.

[28] B. M. Tutolo, A. J. Luhmann, X.-Z. Kong, M. O. Saar, and W. E. Seyfried, "CO_2 sequestration in feldspar-rich sandstone: Coupled evolution of fluid chemistry, mineral reaction rates, and hydrogeochemical properties," *Geochimica et Cosmochimica Acta*, vol. 160, pp. 132–154, 2015.

[29] N. Wei, M. Gill, D. Crandall et al., "CO_2 flooding properties of Liujiagou sandstone: Influence of sub-core scale structure heterogeneity," *Greenhouse Gases: Science and Technology*, vol. 4, pp. 400–418, 2014.

[30] W. B. Fei, Q. Li, X. C. Wei et al., "Interaction analysis for CO_2 geological storage and underground coal mining in Ordos Basin, China," *Engineering Geology*, vol. 196, pp. 194–209, 2015.

[31] Q. Zhu, D. Zuo, S. Zhang et al., "Simulation of geomechanical responses of reservoirs induced by CO_2 multilayer injection in the Shenhua CCS project, China," *International Journal of Greenhouse Gas Control*, vol. 42, pp. 405–414, 2015.

[32] Q. Li, H. Shi, D. Yang, and X. Wei, "Modeling the key factors that could influence the diffusion of CO_2 from a wellbore blowout in the Ordos Basin, China," *Environmental Science and Pollution Research*, vol. 24, pp. 3727–3738, 2017.

[33] D. Liu, Y. Li, S. Song, and R. Agarwal, "Simulation and analysis of lithology heterogeneity on CO_2 geological sequestration in deep saline aquifer: a case study of the Ordos Basin," *Environmental Earth Sciences*, vol. 75, pp. 1–13, 2016.

[34] T. Xu, E. Sonnenthal, N. Spycher, and K. Pruess, "TOUGHREACT—A simulation program for non-isothermal multiphase reactive geochemical transport in variably saturated geologic media: Applications to geothermal injectivity and CO_2 geological sequestration," *Computers & Geosciences*, vol. 32, pp. 145–165, 2006.

[35] T. Xu, N. Spycher, E. Sonnenthal, L. Zheng, and K. Pruess, "TOUGHREACT user's guide: a simulation program for non-isothermal multiphase reactive transport in variably saturated geologic media, Version 2.0," Earth Sciences Division, Lawrence Berkeley National Laboratory University of California, Berkeley, CA, USA, 2012.

[36] K. Pruess, C. Oldenburg, and G. Moridis, "TOUGH2 user's guide, Version 2.0," Lawrence Berkeley Laboratory Report LBL-43134, Berkeley, CA, USA, 1999.

[37] N. Spycher and K. Pruess, "CO_2-H_2O mixtures in the geological sequestration of CO_2. II. Partitioning in chloride brines at 12–100∘C and up to 600 bar," *Geochimica et Cosmochimica Acta*, vol. 69, pp. 3309–3320, 2005.

[38] T. J. Wolery, "Software package for geochemical modeling of aqueous system: Package overview and installation guide (version 8.0)," Lawrence Livermore National Laboratory Report UCRL-MA-110662 PT I, Livermore, California, USA, 1992.

[39] L. André, M. Azaroual, and A. Menjoz, "Numerical simulations of the thermal impact of supercritical CO_2 injection on chemical reactivity in a carbonate saline reservoir," *Transport in Porous Media*, vol. 82, pp. 247–274, 2010.

[40] Y. Wang, *The Research Report of the Shenhua 0.1 Mt CCS Demonstration Project*, The Appraisal Meeting of the Shenhua 0.1 Mt CCS Demonstration Project, Ordos, China, 2014.

[41] M. T. van Genuchten, "A closed-form equation for predicting the hydraulic conductivity of unsaturated soils," *Soil Science Society of America Journal*, vol. 44, no. 5, pp. 892–898, 1980.

[42] A. T. Corey, *The Interrelation between Gas and Oil Relative Permeabilities*, 1954.

[43] H. Wang, "Study on the interaction of CO_2 fluid with sandstone in Shiqianfeng," *Jilin University*, 2012.

[44] X. Yang, *Experimental study of CO_2 fluid on the geological transformation of reservoir sandstone. In*, Jilin University, 2012.

[45] Y. Tao, *Experimental study on the interaction of CO_2/CO_2-H_2S fluid with sandstone in Liujiagou*, Jilin University, 2013.

[46] T. Xu, J. A. Apps, and K. Pruess, "Numerical simulation of CO_2 disposal by mineral trapping in deep aquifers," *Applied Geochemistry*, vol. 19, pp. 917–936, 2004.

[47] T. Xu, J. A. Apps, and K. Pruess, "Mineral sequestration of carbon dioxide in a sandstone-shale system," *Chemical Geology*, vol. 217, pp. 295–318, 2005.

[48] W. Zhang, Y. Li, T. Xu et al., "Long-term variations of CO_2 trapped in different mechanisms in deep saline formations: A case study of the Songliao Basin, China," *International Journal of Greenhouse Gas Control*, vol. 3, no. 2, pp. 161–180, 2009.

[49] G. Yang, Y. Li, X. Ma, and J. Dong, "Effect of chlorite on CO_2-water-rock interaction," *Earth Science—Journal of China University of Geosciences*, vol. 39, pp. 462–472, 2014.

[50] Y. Wan, *Migration and transformation of CO_2 in CO_2geological sequestration process of Shiqianfeng saline aquifers in Ordos Basin*, Jilin University, 2012.

[51] T. Xu, Y. K. Kharaka, C. Doughty, B. M. Freifeld, and T. M. Daley, "Reactive transport modeling to study changes in water chemistry induced by CO_2 injection at the Frio-I Brine Pilot," *Chemical Geology*, vol. 271, pp. 153–164, 2010.

[52] C. T. Gomez, J. Dvorkin, and T. Vanorio, "Laboratory measurements of porosity, permeability, resistivity, and velocity on Fontainebleau sandstones," *Geophysics*, vol. 75, pp. 191–204, 2010.

[53] A. S. Ziarani and R. Aguilera, "Pore-throat radius and tortuosity estimation from formation resistivity data for tight-gas sandstone reservoirs," *Journal of Applied Geophysics*, vol. 83, pp. 65–73, 2012.

[54] Z. Yan and Z. Zhang, "The effect of chloride on the solubility of calcite and dolomite," *Hydrogeology & Engineering Geology*, vol. 36, pp. 113–118, 2009.

[55] L. Xiao and S. Huang, "Model of thermodynamics for dissolution of carbonate and its geological significances," *Journal of Mineralogy & Petrology*, vol. 23, pp. 113–116, 2003.

[56] Z. Yan, H. Liu, and Z. Zhang, "Influences of temperature and P_{CO_2} on the solubility of calcite and dolomite," *Carsologica Sinica*, vol. 28, pp. 7–10, 2009.

[57] S. M. Amin, D. J. Weiss, and M. J. Blunt, "Reactive transport modelling of geologic CO_2 sequestration in saline aquifers: The influence of pure CO_2 and of mixtures of CO_2 with CH_4 on the sealing capacity of cap rock at 37 degrees C and 100 bar," *Chemical Geology*, vol. 367, pp. 39–50, 2014.

[58] F. Liu, P. Lu, C. Zhu, and Y. Xiao, "Coupled reactive flow and transport modeling of CO_2 sequestration in the Mt. Simon sandstone formation, Midwest U.S.A," *International Journal of Greenhouse Gas Control*, vol. 5, pp. 294–307, 2011.